Table 1. Comparison with previous photometries of Walker (1992a) and Alcaino et al. (1990). The errors on the mean are quoted; the standard deviation of the data are 0.05 mag in $V$and 0.06 in $(V–I)$ for the Alcaino sample, and 0.04 mag in V for the Walker sample.

Ref.	$V–V_{\rm ref}$	$(V–I)–(V–I)_{\rm ref}$
Alcaino et al. (1990)	0.012 ± 0.004	0.035 ± 0.004
Walker (1992a)	0.001 ± 0.001	

A. Observations and reductions

A.1. Instrumental magnitudes

The journal of the observations is reported in Table 1 of the main text. V and I images have been obtained during two nights in 1993 February at the ESO 3.5 m NTT with EMMI at the Nasmyth focus. The scale is 0.″44/px and the size of the chip is 1024 × 1024 px^2, which gives a square field 7.′5 wide. With nine fields, we mapped a region of ≃ 15.5 arcmin in radius around the cluster centre, as shown in Fig. 1 of the main text.

Two further images were secured on 1993 December 10 in order to have a comparison background field. The frames are centred 30′ east of NGC 1851, and cover 9.6′ × 7.4′ , with a scale of 0.″34/px.

The image processing has been performed in part with MIDAS and in part with IRAF; photometry has been completed at the *Instituto de Astrofísica de Canarias* (IAC) with DAOPHOT II (Stetson 1987, 1994) in the IRAF implementation. A quadratic dependence of the PSF with radius was necessary to account for off-axis aberrations and the best-fitting analytic function was found to be a Moffat ($\beta = 2.5$) function.

A.2. Calibration of standard system

Let us call m_1 and m_2 the aperture magnitudes of a star in the fields 1 and 2; we can remove the dependence on the local exposure conditions by normalizing each magnitude according to the relation

$$\overline{m} = m + 2.5\,\log(t + \delta\,t) - k_m\,X,$$

where t and $\delta\,t$ are the exposure time and the shutter delay, k_m is the extinction coefficient and X is the air mass. For each star in the overlap area of any two fields we expect $\overline{m}_1 - \overline{m}_2 = 0$, mean value. In turn, we actually have PSF magnitudes. The corrections to aperture magnitudes have been found assuming that $m = m^{\rm PSF} + \Delta$ (Stetson 1987) and computing the mean offsets on a set of bright isolated objects. The difference in normalized magnitudes for the same star in two overlapping fields can therefore be written as:

$$\overline{m}_1 - \overline{m}_2 = (m_1^{\rm PSF} - m_2^{\rm PSF}) + (\Delta_1 - \Delta_2)$$
$$+2.5\,\log(t_1 + \delta\,t_1)/(t_2 + \delta\,t_2) - k_m\,(X_1 - X_2).$$

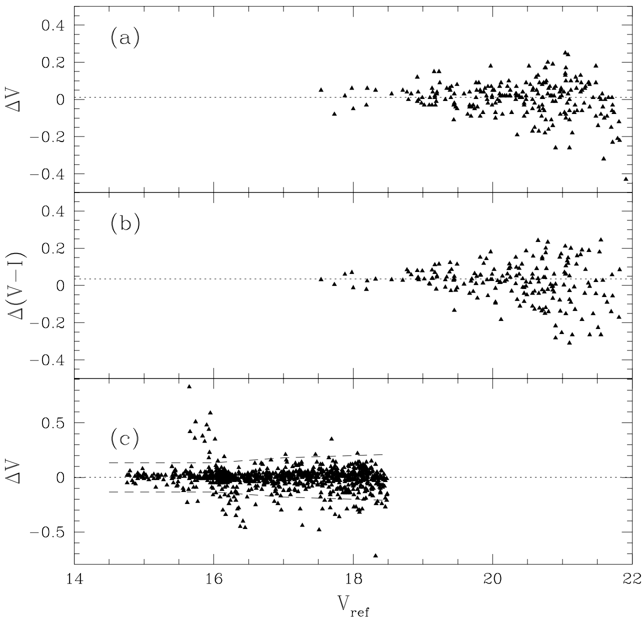

Fig. 1. Plot of the photometric zero-point differences: dotted lines are the means reported in Table 1; panels (a) and (b) refer to Alcaino et al. (1990); panel (c) refers to Walker (1992a). The differences are in the sense *this paper–reference*

The observed scatter of the mean $< \overline{m}_1 - \overline{m}_2 >$ around the zero point then gives a measure of the internal uncertainties arising from all sources of error (aperture corrections, exposure times and delays, and air masses). Comparing the 8 external fields to the central one we find $< \overline{v}_1 - \overline{v}_2 >= 0.029 \pm 0.015$ and $< \overline{i}_1 - \overline{i}_2 >= 0.009 \pm 0.018$; the central $\overline{v}$ and $\overline{i}$ magnitudes plus the quoted offsets have then been taken as the instrumental zero-point, with 1–σ uncertainties of 0.015 mag in v and 0.018 mag in i.

Next, the above $\overline{v}$ and $\overline{i}$ instrumental magnitudes have been corrected to the standard VI system, making use of the following relations:

$$V = v + 0.04(V - I) - 0.84$$
$$I = i - 0.01(V - I) - 1.51$$

The numerical coefficients have been obtained by Veronesi (1995), from the observations of eight Landolt (1992) standard stars in the same observing run. The calibration uncertainty is estimated 0.03 mag in V and 0.02 mag in I, so the total zero-point error is $\sigma_V = 0.03$ mag and $\sigma_I = 0.03$ mag, obtained adding the latter errors to the internal uncertainties.

We have compared our photometry with other photometric data in the literature. Figure 1 shows the comparison with Walker (1992a, 956 common stars) and Alcaino et al. (1990, 236 common stars); Table 1 gives the zero-point differences and it can be seen that a general agreement exists to within a few 0.01 mag, although there is a notable dispersion in the data.

An interesting feature of Fig. 1 is the stars in panel (c) at $V = 16.0 \pm 0.5$ mag and falling outside the 3-σ dispersion strip (dashed lines). There are $\sim$ 30 such stars: 14 are known RR Lyr (Liller 1975; Wehlau et al. 1978; Wehlau et al. 1982). The remaining $\sim$ 20 objects are candidate new RR Lyr variables or anomalous stars and are discussed in Sect. 3.5.

Almost all the objects marked with open and filled squares in Fig. 7 have $\Delta V_{\rm Walker} < 0$ mag, i.e. they are systematically brighter in our photometry (cf. also panel (c) in Fig. 1): the figure also shows that these objects are just above the V photometric limit of the W92 diagram (dotted line), so we suspect that the observed discrepancies are due to a systematic error at the limit of W92 photometry. This is further confirmed by the fact that, apart from one case, stars for which $\Delta V_{\rm Walker} > 0$ mage are all above $V = 17.9$ mag (filled squares in Fig. 7).

A systematic error in the W92 photometry is also our suggested explanation for the four blue objects in Fig. 7 marked with open triangles. These are all at the inner radial limit of the W92 CMD ($\simeq$ 25 arcsec), i.e. where the problems of blending become severe. Moreover, stars 8, 9 and 10 are part of the objects $\sim$ 0.4 mag bluer than the BHB in the W92 CMD, while they fall at the "right" position within our BHB.

A.3. Calibration of the background field

Eight standard stars from Landolt (1992) were used to calibrate the background field; we only needed to calibrate the V frames, since the calibration of the I band is available in Zoccali et al. (1997). The magnitudes determined within an aperture of 6.8$''$ have been compared to the standard values, after the following normalization:

$$m_{\rm norm} = m_{\rm local} + 2.5 \log t_{\rm exp} - k_{\rm m}\, X. \qquad \text{(A1)}$$

The extinction coefficient $k_V = 0.121$ has been provided by Geneva Observatory. Figure 2 shows the quantity $(V - V_{\rm norm})$ as a function of the $(V-I)$ colour, and a linear fit yields

$$V = v_{\rm norm} + 0.029\,(V-I) - 0.040$$

with a residual dispersion of 0.004 mag (rms). Similarly, Zoccali et al. for the I band find

$$I = i_{\rm norm} - 0.004\,(V-I) - 0.604$$

For the background field magnitudes, an aperture correction $\Delta m^{\rm PSF}_{\rm local}$ of 0.20 mag and 0.24 mag has been applied for the V and I bands, respectively. These values have been determined using a set of $\sim$ 10 isolated and bright stars, and all aperture magnitudes have been measured within an aperture of 6.8$''$: we checked that outside this aperture the magnitudes are seeing independent. Finally, the values of $t_{\rm exp}$ and X used for the V and I frames are 120 s, 180 s and 1.443, 1.403 respectively.

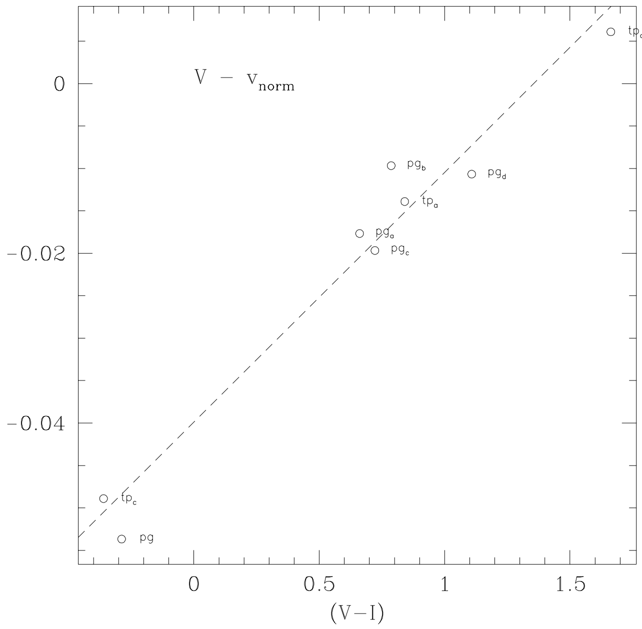

Fig. 2. The quantity $(V - v_{\rm norm})$ $(V = V_{\rm Landolt(1992)})$ as a function of the standard-star colour $(V-I)$; the straight line represents the adopted calibration: $V = v_{\rm norm} + 0.029\,(V-I) - 0.040$ with a residual dispersion of 0.004 mag (rms). The $v_{\rm norm}$ magnitudes have been computed from the instrumental aperture magnitudes and normalized according to Eq. A1.

A.4. Completeness and photometric errors

Completeness at the various magnitude levels has been computed by adding artificial stars to the original frames and checking what percentage is recovered, after a reduction stage equivalent to that of the original images. Completeness within the CMD is evaluated considering only those stars identified both in the V and I frames. One major complication with clusters of high concentration such as NGC 1851 is that completeness is a function not only of the magnitude but also of the radial position of the stars. While this could be of minor importance for bright stars except into the very centre of the cluster, the probability of finding faint stars in the inner regions is a strong function of the radius. Crowding experiments were then carried out for a suitably fine grid of magnitudes and radii, and completeness has been linearly interpolated where no mesh points were available.

In Fig. 3, the dependence of completeness both on radius and V magnitude is shown for the central field, where the completeness gradient is most evident: this figure clearly shows that the 50% level is reached at different radii for different magnitudes (dotted curve). This curve is well fitted by the line $V_{50\%} = 0.036\, r + 16.82$; similarly, it is found $I_{50\%} = 0.037\, r + 15.89$.

The evaluation of completeness also allows checking the internal photometric errors, simply by comparing out-

Table 2. Photometric errors as a function of magnitude.

V	I	off V	off I	σ_V	σ_I	σ_{V-I}
16.74	15.78	0.007	0.000	0.01	0.03	0.04
17.24	16.32	0.000	0.000	0.03	0.03	0.04
17.74	16.84	0.008	0.015	0.02	0.03	0.03
18.74	17.86	0.008	0.013	0.04	0.03	0.05
19.23	18.53	0.007	0.002	0.03	0.03	0.04
19.52	18.79	0.018	0.019	0.05	0.06	0.08
19.73	19.05	0.009	0.008	0.05	0.04	0.07
19.80	19.10	0.017	0.015	0.06	0.05	0.08
20.02	19.31	0.018	0.016	0.05	0.05	0.07
20.23	19.52	0.014	0.015	0.05	0.07	0.09
20.52	19.78	0.014	0.010	0.06	0.05	0.08
20.99	20.23	0.018	0.010	0.06	0.08	0.10
21.02	20.24	0.017	0.017	0.07	0.07	0.10
21.50	20.57	0.010	0.095	0.08	0.11	0.13
22.00	21.07	0.021	0.028	0.10	0.12	0.16
22.03	21.07	0.030	0.023	0.14	0.12	0.19
22.54	21.43	0.034	0.022	0.16	0.14	0.21
23.04	21.74	0.102	0.042	0.17	0.15	0.23
23.51	22.23	0.153	0.041	0.20	0.18	0.27

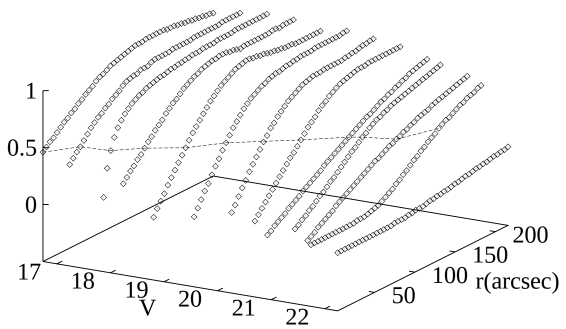

Fig. 3. Completeness as a function of magnitude and radius for the central field.

put magnitudes to the magnitudes of the artificial stars; besides adding a random scatter, reduction also introduces an offset, as can be seen in Table 2 (offsets are labeled *off V* and *off I* in this table, and correspond to *off* $m = m_{\rm in} - m_{\rm out}$); these are in the sense that the recovered magnitudes are always brighter than the added ones, as expected (Stetson 1987). Errors and offsets increase vs. magnitude, but keep within a few 0.01 mag to the very limit of our photometry.

B. *HST* data

The compactness of NGC 1851 prevents the study of its central regions with ground-based instruments. We then searched the *HST* archives through STARVIEW and found that ten images of NGC 1851 were available: two of them (see Table 2) are WFPC/I 160 sec exposures in the F785LP and F555W filters (which closely match the I and V colours).

Technical details about WFPC/I can be found in *HST* user manuals: this camera consists of four 800 × 800 px CCDs (CCD nr. 5 to 8), which subtend an area of 70.4 × 70.4 arcsec^2 on the sky (due to the gaps between adjacent chips, the effective area is 68 × 68 arcsec^2). The scale is $0''.0439$/px, the read-out noise is reported to be 13 e^-, with a conversion factor of 7.6 e^-/ADU. Saturation takes place below 4095 ADU, the actual value depending on the current flat-fielding. A histogram of the intensity distribution, revealed that in our case saturation occurs at ∼ 3600 ADU for the F555W filter, and at ∼ 3200 ADU for the F785LP filter. The most relevant bad features are many dead columns/rows across the surface of the chips, which have been removed.

Stellar photometry has been performed again with DAOPHOT II, and we limited ourselves to the PC field, covering the inner ∼ 30″× 30″ of the cluster. First we simply tried to derive aperture magnitudes within a 1 px radius, i.e. within the central sharp peak which comprises 10% of the energy: it has been shown (Gilmozzi 1990; Ortolani & Murtagh 1992) that aperture photometry of the central $0''.1$ of the PSF, gives satisfactory results for the WFPC1. The major complication was that a very high detection threshold had to be set in order to avoid contamination from PSF artefacts: there are so many misidentifications that our cross-matching program failed to join the two colour tables. We then performed PSF photometry by means of ALLSTAR, which provides a check on the input list of objects and helps reject many spurious detections; we simply chose a Gaussian PSF function, which is adequate for this purpose. Finally, simple aperture photometry has been performed on the resulting catalogue, which comprises ∼ 1900 objects.

Reduction of the *HST* material has been accomplished with the main purpose of checking radial trends in the HB populations in the inner part of the cluster; we just need to distinguish between the red and blue part of the HB, so absolute calibration is not required. However, for the aim of comparing the two data sets, we made a simple calibration: as there are no stars in common with the calibrated catalogue, since the PC field falls in a region where the completeness of the NTT/EMMI data goes almost to zero, we chose three significant points within the two CMDs and found the transformation parameters, assuming linear relations. The relations may then be written as follows:

$$V - I = 0.81\ (\mathrm{F555W - F785LP}) + 0.01\ \mathrm{F785LP} + 1.40$$
$$I = 0.14\ (\mathrm{F555W - F785LP}) + 1.00\ \mathrm{F785LP} - 2.70$$

Figure 8 (lower panel) shows the *HST*-calibrated CMD, together with a plot of the fiducial points for the

NTT/EMMI set: the overlap is quite satisfactory for the purposes of the present paper.

References

Gilmozzi R. 1990, Space Telescope Instrument Science Report WFPC 90-007

Ortolani S., Murtagh F. 1992, *ST-ECF Newsl.*, No. 17, 5

Stetson P.B. 1994, PASP 106, 250

Veronesi C. 1995, Masters Thesis in Astronomy, Univ. of Padova, Italy

Zoccali M., Piotto G., Zaggia S.R., Capaccioli M. 1998, A&A, accepted

This article was processed by the author using Springer-Verlag LaTeX A&A style file *L-AA* version 3.